PROCEEDINGS OF SCIENCE

DArk Matter Particle Explorer: 7 years in Space

Andrii Tykhonov[a,*] **(for the DAMPE collaboration)**

[a] *Department of Nuclear and Particle Physics, University of Geneva, 24, quai Ernest-Ansermet, CH-1205 Genève 4, Switzerland.*

E-mail: andrii.tykhonov@cern.ch

The DArk Matter Particle Explorer (DAMPE) is a pioneering calorimetric experiment that has been successfully operating in space since December 2015, designed to detect cosmic rays up to unprecedentedly high energies thanks to the fine-grained thick BGO calorimeter and relatively large geometric factor. Among the scientific goals of DAMPE are the precise measurements of cosmic-ray electron plus positron spectrum, including the detection of possible indirect dark matter signatures, spectral measurements of primary and secondary cosmic-ray species, and gamma-ray physics. For electrons and gamma rays, it covers an energy range from GeV to about 10 TeV, with an outstanding energy resolution close to 1%. Proton and ion cosmic rays can be measured up to hundreds of TeV in kinetic energy. In this contribution, we first give an overview of the DAMPE mission and its on-orbit operation status. Then, we highlight the key scientific results, including the measurements of the BCNO group, boron-to-carbon ratio, proton plus helium spectrum beyond 100 TeV, gamma-ray physics and more. Finally, the ongoing efforts for lepton, light, and heavy hadron cosmic rays are briefly discussed along with the new data analysis techniques.

38th International Cosmic Ray Conference (ICRC2023)
26 July - 3 August, 2023
Nagoya, Japan

*Speaker

https://pos.sissa.it/

PoS(ICRC2023)003

1. Introduction

DAMPE (DArk Matter Particle Explorer) is a satellite-borne cosmic- and gamma-ray detection instrument that was developed by an international collaboration of Chinese, Swiss and Italian institutes [1]. It was successfully launched in space in December 2015 from the Gobi desert in China, operating on a 500 km sun-synchronous orbit in sky survey mode. The instrument demonstrates extremely smooth performance since launch until the present moment, accumulating about two billion cosmic-ray events and about 40 thousand gamma-ray events per year.

DAMPE is designed to encompass a broad scientific program: measurement of cosmic-ray electron plus positron spectrum up to about 10 TeV along with the possible detection of dark matter annihilation or decay signatures in it; measurement of individual hadronic cosmic-ray spectra, from proton to iron and beyond, with kinetic energies up to hundreds of TeV; measurement of diffuse gamma-ray spectrum and study of gamma-ray sources. The detector features unprecedented energy resolution for electrons and photons, about 1% at 100 GeV and higher energies, and about 10–30% for hadronic cosmic rays. The mission aims to shed light on key fundamental problems: the origin of cosmic rays, its acceleration and propagation mechanisms; precise composition of cosmic-ray components close to the "knee"; identification of possible contribution of dark matter or, alternatively, local accelerators in cosmic rays. The list is far from being exhaustive. As of now, DAMPE has delivered spectral measurements of leptonic and hadronic cosmic-ray species, ranging from electrons, protons, and helium to carbon and oxygen, reaching unparalleled high energies for direct detection experiments. Thanks to its excellent energy resolution, the DAMPE mission also keeps providing intriguing insights into gamma-ray and solar physics.

A series of physics results have been published by DAMPE, along with the new results presented for the first time at this conference. A condensed summary of those is provided in this contribution. The paper is structured as follows. First, in section 2 we give an overview of the DAMPE instrument and its base characteristics. In section 3 we present the on-orbit status of DAMPE and its major components. The main part of this contribution is dedicated to physics results and ongoing analysis activities, reviewed in section 4. Finally, a short summary is provided in section 5.

2. The DAMPE instrument

The DAMPE payload consists of four sub-detectors (Figure 1), from top to bottom following the path of a cosmic/gamma ray: the Plastic Scintillator Detector array (PSD) serves as a cosmic-ray absolute charge measuring device and provides a veto signal for the gamma-ray identification [2]; the Silicon–tungsten TracKer–converter (STK) measures the cosmic-ray trajectory and the absolute charge, while promoting the conversion of gamma rays into electron–positron pairs, for the identification of gamma-ray's incoming direction [3]; the Bismuth Germanium Oxide (BGO) calorimeter is the core sub-detector of DAMPE – with about $32X_0$ (radiation lengths) thickness it provides precise cosmic- and gamma-ray energy measurements and features a proton rejection power of about 10^4 for cosmic-ray electron identification [4]; in the lowermost part of DAMPE, a boron doped plastic scintillator is installed – the NeUtron Detector (NUD), which serves as an additional proton rejection tool [5]. A more detailed description of DAMPE sub-detectors in the context of their in-flight operation is provided in the next section.

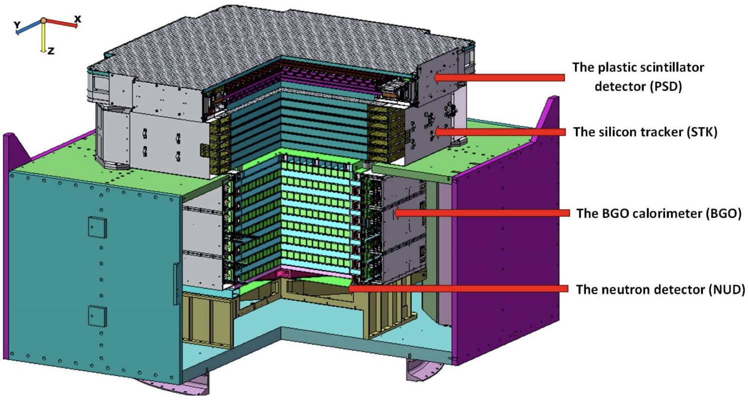

Figure 1: Schematic view of the DAMPE detector. Figure from [1].

The DAMPE payload weights about 1.3 tonnes with a total power consumption of about 130 W. The rate of data transmission to the ground is about 12 GB/day [1]. To optimise the instrument and assist in data analysis, the DAMPE detector is mimicked in a comprehensive simulation model [6, 7], implemented in the GEANT4 package [8]. An alternative FLUKA [9] simulation model was also implemented, for cross-validation while assisting towards the estimation of systematic uncertainties in the data analysis.

The instrument energy response is calibrated in the beam test campaigns at CERN Proton/Super-Proton Synchrotron accelerators (PS/SPS), with beam energies ranging from a few GeV to about 250 GeV and 400 GeV for electron and proton beams, respectively. For ions, tests with mixed composition beams of 40 GeV/n and 75/n were performed [4]. The energy scale is also validated on-orbit using the geomagnetic cut-off of a cosmic ray spectrum, theoretically calculated for different cosmic-ray species, and confirmed with the observed DAMPE data [10, 11]. The energy scale estimated on orbit is in very good agreement with ground-based calibrations, with a residual observed difference conservatively smaller than 2% [11]. In addition, a study of BGO fluorescence quenching has been done with beam-test and flight data [12, 13], along with the dedicated laser excitation tests of the BGO crystals [14]. The aforementioned tests showed that the BGO quenching affects the energy scale of light hadronic cosmic rays at low energies, about 10 GeV, by a few percent. At the same time, the impact on cosmic-ray electrons [14] has been confirmed to be negligible.

3. Status of DAMPE on orbit

All sub-detectors of DAMPE show stable operation since launch. Regular monitoring and re-calibration is done on orbit in order to ensure the optimal instrument performance. Below we provide a very brief description of the key sub-detectors and report their in-flight monitoring metrics.

3.1 BGO calorimeter

The DAMPE calorimeter consists of 14 layers of BGO bars, $25\times25\times600$ mm^3, 7 layers in x direction and 7 in y direction, in a hodoscopic arrangement. Scintillation light produced by particle interactions in BGO is collected by photomultipliers on both ends of each bar. The readout is

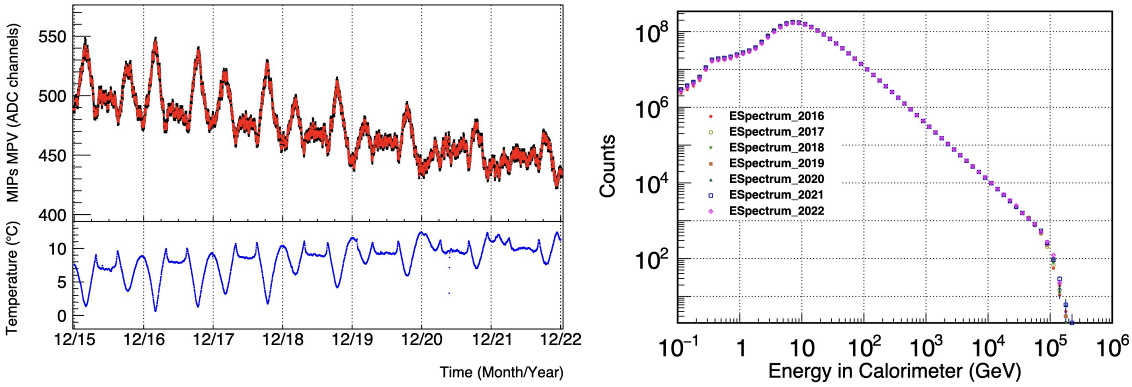

Figure 2: Left: average MPV of a proton MIP in a BGO bar and average temperature of BGO bars as a function of time. Right: all-particle deposited energy spectrum for different years.

designed to maintain a wide dynamic range of energies, from 10 MeV to 2 TeV per bar [4]. This is possible thanks to a multi-dynode configuration with dynodes 2, 5, and 8 corresponding to low, middle, and high gain, respectively.

On-orbit behaviour of the calorimeter can be influenced by a few factors, the major ones being the temperature variation and the ageing of BGO crystals. To account for those, the energy scale calibration is performed at every DAMPE orbit through measuring the Most Probable Value (MPV) of a proton signal that passes through BGO without creating a hadronic shower, hereafter referred to as Minimum Ionising Particle (MIP). Figure 2 (left) shows the MPV behaviour as a function of time along with the corresponding temperature variation, where a clear correlation between the two can be observed. The annual oscillation of temperature is driven by the corresponding variation of the DAMPE orbit inclination with respect to the Sun. The trend of the slightly increasing temperatures over the years can be explained by the ageing of the satellite's thermal insulation materials. The decrease in the average MPV is due to the deterioration of light transmittance in BGO material caused by the long-term exposure to cosmic radiation. The average increase of the light attenuation since the start of the mission is about 10% – taken into account thanks to the regular BGO calibration. Figure 2 (right) shows the deposited BGO energy for different years. The stability of energy scale after calibration is better than 1%.

3.2 Plastic Scintillator Detector (PSD)

The PSD detector consists of two double-layers of plastic scintillator bars, one along the x axis and the other along the y axis, each equipped with 41 bars of the dimension $10{\times}28{\times}884$ mm^3 ($10{\times}25{\times}884$ mm^3 for the bars at edges). To ensure optimal charge reconstruction, multiple calibrations are performed, including the light attenuation correction [15], quenching equalisation [16] and geometrical alignment [17]. The first two corrections take into account the attenuation of light depending on the impinging particle position in a PSD bar and quenching of light yield for high ionisation signals [18], respectively. The accurate geometrical alignment, in turn, allows to reconstruct sharper charge distributions thanks to the precise knowledge of the particle path length in a PSD bar (Figure 3 left). Similar to the BGO, regular monitoring and calibration with the proton MIP signals is performed, resulting in a stable charge reconstruction (Figure 3 right).

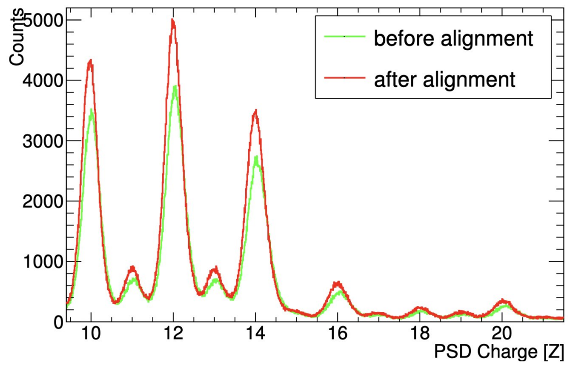

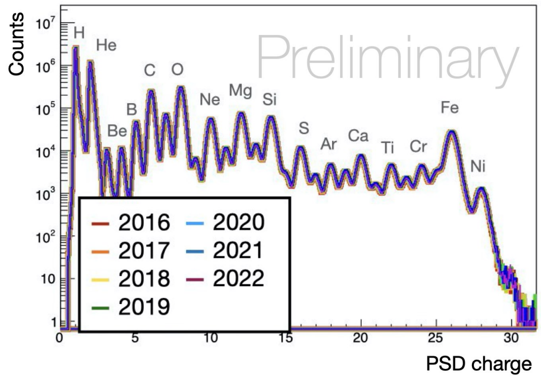

Figure 3: Left: comparison of PSD charge spectrum with and without the alignment correction (figure from [17]). Right: all-particle charge spectrum for different years.

3.3 Silicon–tungsten TracKer Converter (STK)

The STK detector consists of 12 layers of single-side silicon-strip detectors, 6 in x and 6 in y directions, respectively, interleaved with three layers of tungsten plates (1 mm each) for the photon conversions. The silicon sensors are assembled in ladders, 4 sensors per ladder daisy-chained via micro-wire bonds. The total silicon area is about 6.6 m^2. The silicon strip pitch is 121 μm with every other strip read out by VA ASIC chips [3]. STK has the highest data throughput in DAMPE, amounting to a total of 73728 channels.

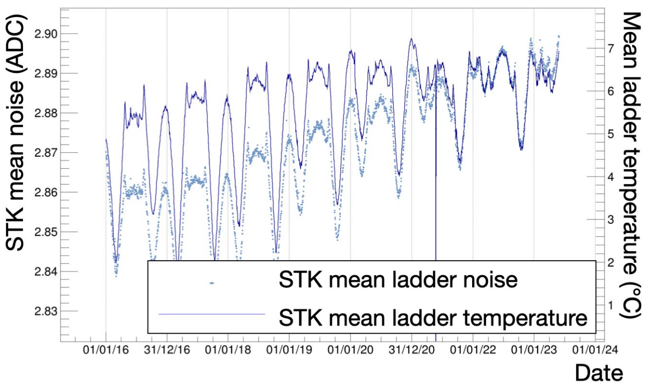

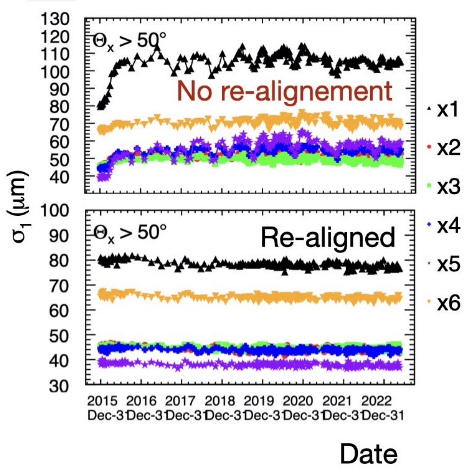

Figure 4: Left: average STK noise and ladder temperature as a function of time. Right: difference between observed hit positions and the ones predicted from the track (unbiased residuals) in different x layers of the STK at high incidence angle; two cases are shown: without (top) and with (bottom) the regular re-alignment.

One of the key metrics of the STK performance is the level of readout noise [19]. Figure 4 (left) shows the comparison of average STK noise as a function of time together with the average ladder temperature. The noise behaviour is correlated with the temperature variations and changes marginally in the range between ~2.84 and ~2.9 ADC counts. Given that the average MIP signal for protons impinging on a readout strip is ~50 ADC counts, the observed noise variations are fully negligible for the data analysis [3]. The total number of channels with the abnormal noise (exceeding a threshold of 5 ADC counts) is less than 0.3% and remains stable with time. To ensure optimal particle trajectory and position reconstruction, regular re-alignment is performed every two weeks and applied at the data reconstruction stage [20]. As a result, the position resolution is maintained at the optimal level, and is stable with time (Figure 4 right).

4. Scientific results and prospects

4.1 Electron

Due to the high synchrotron radiation, at TeV and higher energies only electrons from sources within 1 kpc can reach us [21]. Hence, Cosmic Ray Electrons (CRE) provide an ideal probe of local astrophysical sources and possible dark matter signatures in cosmic rays. DAMPE has been designed in order to extend direct CRE measurements in space beyond the TeV milestone with unprecedented energy resolution and the largest data statistics. In 2017, the first direct observation of a break in the CRE electron spectrum at about 0.9 TeV was reported by DAMPE (Figure 5 left), based on 1.5 years of data [22]. One of the most challenging aspects of this analysis is the rejection of the overwhelming proton background, since the cosmic ray proton flux exceeds those of electrons by at least 4 orders of magnitude. To tackle this, an electron/proton discriminator was developed, hereafter referred to as ζ, based on the shower shape characteristics, such as the energy fraction in the last layer of the BGO and the aggregate shower spread in all BGO layers. It allowed maintaining the CRE signal selection efficiency higher than 90% up to ~TeV energies, while keeping the proton background low, not more than 2%.

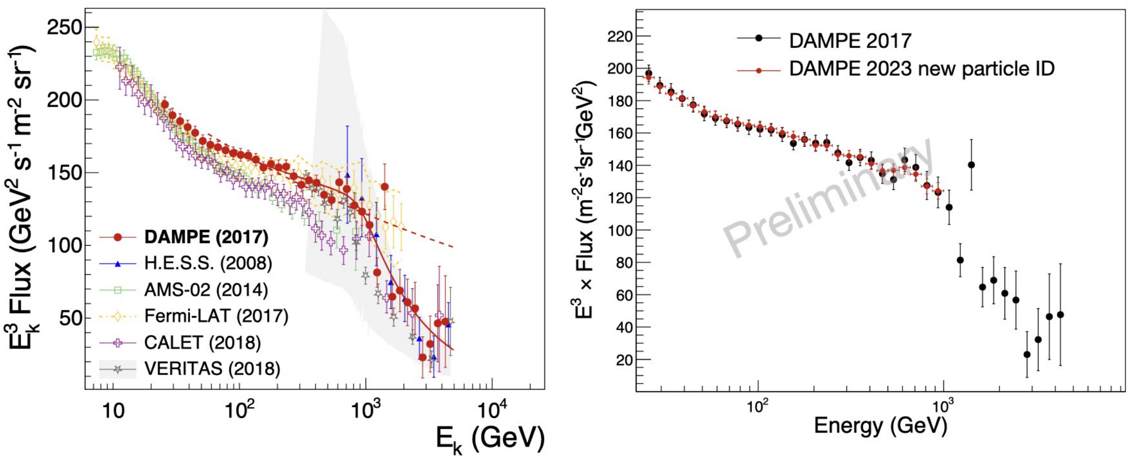

Figure 5: Left: the CRE spectrum (multiplied by E^3) measured by DAMPE [22] and compared with other experiments (see [22] and references therein; data for VERITAS and CALET are taken from [23, 24]. Right: comparison of the CRE spectrum from [22] with the new CRE spectrum (below 1 TeV) calculated using the Neural Network electron/proton classifier [25] based on about 7 years of data.

At higher energies, the proton background substantially increases. Hence, in order to extend the CRE spectrum to about 10 TeV, a more powerful electron/proton discriminator has to be adopted, which is the subject of current research by the collaboration. In particular, recent progress in the application of machine learning techniques to the analysis of DAMPE data shows that Neural Networks (NN) can improve proton rejection by at least factor of 3 at 10 TeV and higher energies [25]. As an alternative, unsupervised techniques such as Principle Component Analysis (PCA) also show very promising results [26]. Finally, while not employed in the original CRE publication, the use of the NUD detector is also investigated, which can further improve the proton rejection power [5]. Overall, said techniques show very good consistency with the more classical analysis based on the ζ variable, in particular in the lower-energy region where the proton background is relatively small (Figure 5 right). This proves that machine learning methods are well suited to facilitate the extension of the CRE spectrum measurement beyond the currently achievable 4.6 TeV. In addition, a possibility is studied for extending the instrument acceptance, though the inclusion of the electrons coming partially from the side of DAMPE [27].

4.2 Proton and Helium

Protons and helium ions are the most abundant primary cosmic-ray species. They allow probing the highest energies that can be reached in cosmic-ray direct detection experiments. The first measurement of the cosmic-ray proton spectrum was published by the collaboration in 2019 [28], confirming the hardening at ~500 GeV, observed previously by the AMS-02 experiment [29], and revealing a new spectral structure – a softening at ∼14 TeV (Figure 6 left). The helium spectrum was then published in 2021 [30], confirming a similar sequence of hardening and softening structures (Figure 6 right) at kinetic energies of ∼1.25 TeV and ∼34 TeV, respectively.

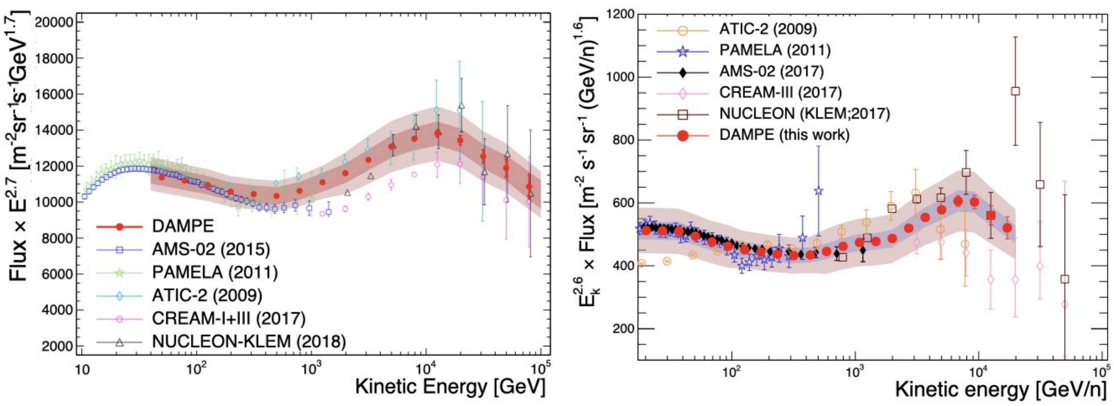

Figure 6: The published cosmic-ray proton (left) and helium (right) spectra, multiplied by $E^{2.7}$ and $E^{2.6}$, respectively. Figures from [28] and [30].

The demonstrated breaks' positions are consistent with the charge-dependent spectral hypothesis, however the mass-dependent hypothesis cannot be excluded. The major source of systematic uncertainties in these measurements is the modelling of hadronic interactions. However, it mostly affects the overall spectrum normalisation, while the spectral features (breaks) are observed consistently regardless of whether the spectral energy unfolding is performed using the GEANT4 [8] or FLUKA [9] package. Another important source of systematics is the particle identification, i. e. the discrimination between proton and helium, and a consequent estimation of the residual background. Furthermore, at particle kinetic energies close to 100 TeV, a saturation of the readout electronics of the BGO calorimeter starts to occur. In order to account for this effect, a dedicated energy correction method was developed [31] and used in the helium analysis [30].

In this conference, a new result has been presented, extending both cosmic ray proton and helium spectra measurements to ∼120 TeV kinetic energy, with 84 and 81 months of data, respectively [32]. The new analyses profit from the machine learning techniques for particle trajectory reconstruction [33] and calorimeter saturation correction [34], recently developed in DAMPE. Thanks to those, particle identification can be performed more precisely in the entire energy range, with reduced systematic uncertainties and substantially increased effective acceptance at the highest energies. The new results confirm the presence of spectral hardening and softening in both helium and proton fluxes. To analyse the spectra we perform the fit procedure as described in [28]. Improved break positions are obtained, thanks to the larger statistics and better particle identification (Figure 7). These results demonstrate that the charge-dependent hypothesis of cosmic-ray spectra is favoured over the mass-dependent one. We are working on the estimation of the significance of this important observation, along with a more in-depth study of the systematic uncertainties.

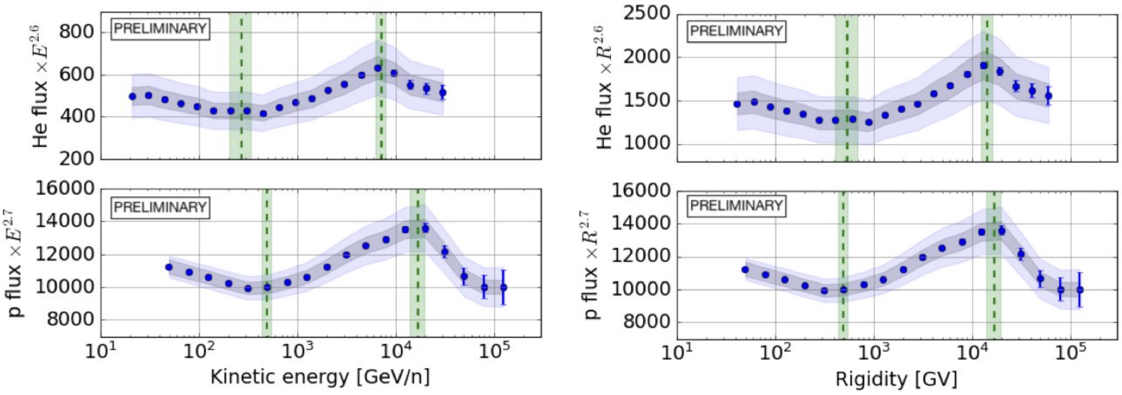

Figure 7: The new (presented at this conference) cosmic-ray proton and helium spectra shown as a function of kinetic energy per nucleon (left) and rigidity (right). The vertical dashed lines indicate the most probable break positions obtained from the fit procedure along with the corresponding uncertainties. Figure from [32].

Finally, we have also performed a combined proton+helium spectrum measurement, submitted for publication earlier this year [35] (Figure 8). While agreeing well with the previously reported individual proton and helium spectra, this analysis extends to a much higher kinetic energy of 316 TeV, thanks to significantly larger combined statistics. Intriguingly, the new results suggest a hint of a new spectral hardening at ∼150 TeV [36], establishing at the same time a strong link between space- and ground-based experiments.

4.3 Lithium, Beryllium, Boron

The analysis of secondary cosmic rays was presented based on 72 months of data [37]. In particular, preliminary results for the boron spectrum were shown (Figure 9a) indicating a presence of a spectral hardening at few hundred GeV per nucleon. Currently, we are working on the in-depth estimation of systematic errors. Apart from the hadronic modelling, one of the dominating uncertainties comes from the estimation of residual backgrounds in the charge selection procedure.

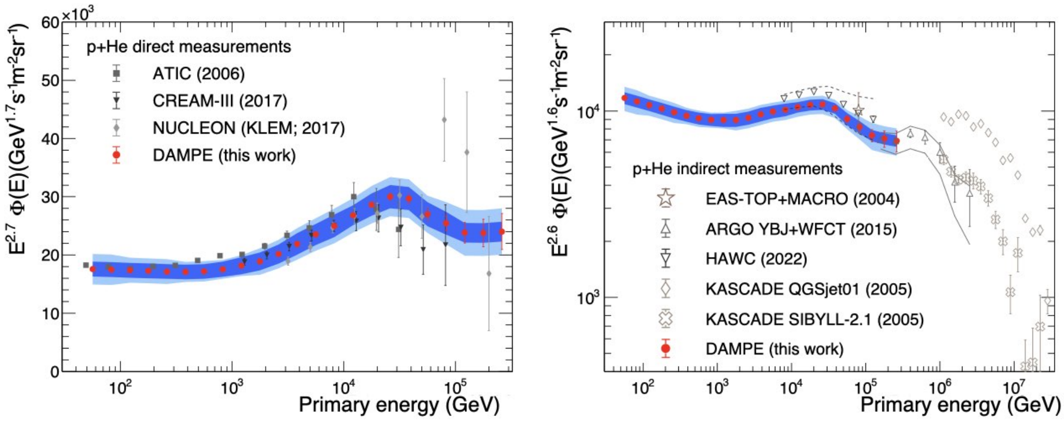

Figure 8: Proton plus helium spectrum based on 6 years of DAMPE data. Figure from [35].

In case of boron, this uncertainty reaches more than 20% at the highest energies [37]. In addition, the estimation of BGO fluorescence quenching and saturation correction is also important for this analysis, as well as for the measurements of other heavier cosmic rays.

4.4 Carbon, Nitrogen, Oxygen

Measurements of cosmic ray carbon and oxygen spectrum were presented [38] (Figure 9b and 9c), confirming, in particular, the hardening structure at a few hundred GeV per nucleon, observed also for the lightest primary cosmic rays (proton and helium). Similar to the analysis of secondary cosmic rays, dominating systematic uncertainties in these measurements come from hadronic modelling (currently not included), and particle identification. An alternative analysis is also underway [39] which utilises the previously developed machine learning techniques for particle tracking and energy reconstruction [33, 34]. It allows increasing the effective acceptance by 20–30% at the highest energies while reducing at the same time the residual background by almost one order of magnitude compared to the conventional analysis. The collaboration is currently working on optimising the particle selection strategy, balancing between classical well-proven techniques and powerful machine learning approach, which requires more validation.

Similar to the case of proton and helium analysis, a combined measurement of carbon-nitrogen-oxygen cosmic rays is also performed (Figure 9d), profiting of a few times larger statistics compared to the individual carbon and oxygen measurements, as well as reduced charge selection uncertainty [40]. The spectrum clearly indicates of a hardening structure, at the same time providing a tentative hint for a possible softening at about 100 TeV.

4.5 Flux ratios

A ratio of secondary-to-primary fluxes provides a unique probe of cosmic-ray propagation mechanisms. Experiment-wise, the ratios also have an advantage of substantially lower uncertainties compared to fluxes themselves, since the majority of systematic errors tend to cancel out in the flux ratio calculation. In 2022, the collaboration has published a measurement of boron-to-carbon (B/C) and boron-to-oxygen (B/O) flux ratios [41], which was also presented at this conference [42]. This result reveals a remarkable hardening structure at ~99 GeV/n (Figure 10). The B/C break is detected at 5.6σ (4.4σ) significance assuming the GEANT4 (FLUKA) hadronic interaction model, while

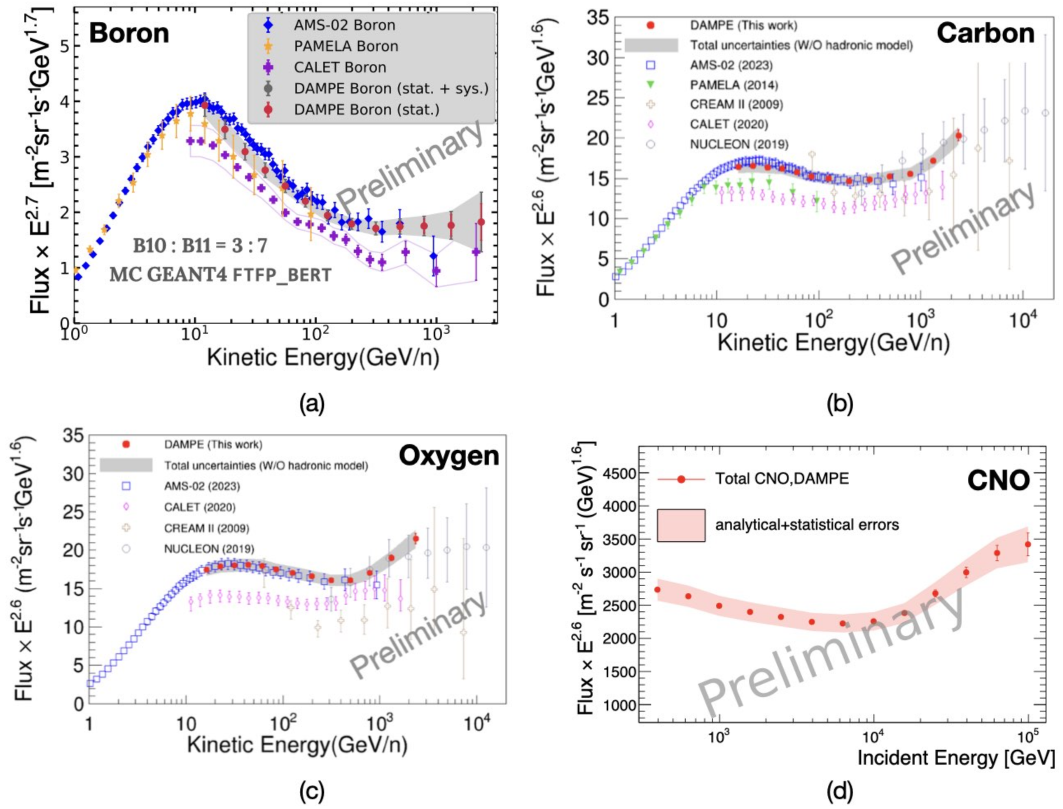

Figure 9: Cosmic ray boron, carbon, oxygen and combined carbon-nitrogen-oxygen spectra presented at the conference. Figures from [37, 38, 40].

the B/O break is observed at 6.9σ significance with either hadronic simulation model. The break possibly indicates the transition from an interstellar turbulence mechanism described by Kraichnan theory [43] to the one predicted by Kolmogorov [44]. Possible explanations could be attributed, for example, to a multiple-component secondary cosmic-ray production [45], or a presence of an unknown primary component on top of a purely secondary one [46].

Next, preliminary measurements of other secondary-to-primary fluxes were presented at the conference: lithium-to-carbon and beryllium-to-carbon, indicating a similar spectral hardening. Additionally, the first preliminary results on secondary-to-secondary flux ratios were presented (Figure 11): lithium-to-boron and beryllium-to-boron [37]. The overestimated (large) error bars in the those results are due to the fact that the systematic uncertainties were extracted directly from the corresponding lithium, beryllium, and boron spectra, without taking into account the error correlation/cancellation. The collaboration is currently working on a profound evaluation of systematic effects, including hadronic modelling, calorimeter quenching and saturation, detailed background estimation, and improved particle reconstruction.

4.6 Heliophysics: Forbush decrease

Forbush Decrease (FD) is a prompt decline in the observed intensity of galactic cosmic rays (GCRs) followed by a gradual restoration, resulting from active solar events, such as coronal mass ejection or solar flares, that swipe low-energy GCRs away from Earth [47]. Various characteristics

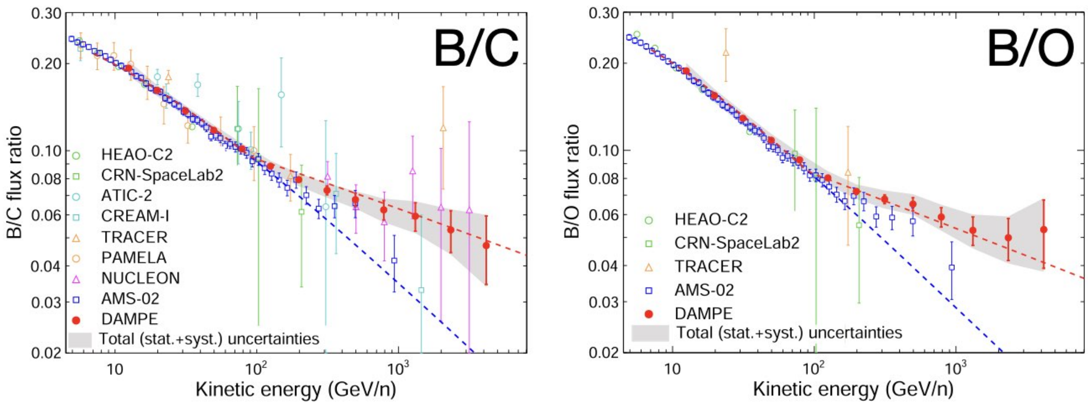

Figure 10: Boron-to-carbon (left) and boron-to-oxygen (right) flux ratios as functions of kinetic energy per nucleon. Figures from [41].

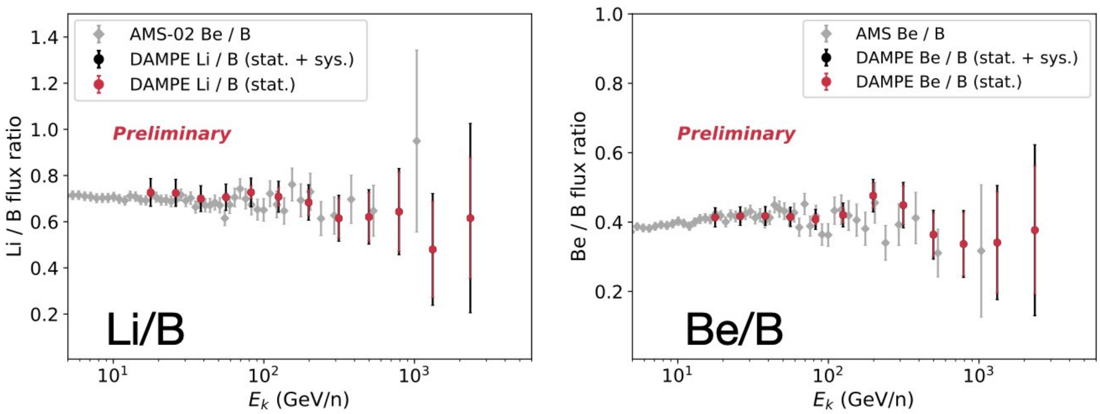

Figure 11: Boron-to-boron (left) and beryllium-to-oxygen (right) flux ratios as functions of kinetic energy per nucleon. Figures from [37].

of FDs have been studied, mostly from the data collected by ground-based Neutron Monitors (NM), which primarily concentrate on secondary neutrons originating from the atmospheric showers. The DAMPE orbit reaches polar regions where the impact of the geomagnetic cut-off is substantially reduced, giving it an opportunity to study FD events from a new perspective. In particular, we focus on the Cosmic-Ray Electron (CRE) spectrum at low energies modulated by FD events (Figure 12 left-hand side panels). In 2021, an article based on one FD event detected by DAMPE in September 2017 was published [48]. Updated (preliminary) results based on 3 FD events (two in 2017 and one in 2021) were presented at this conference [49]. They show that the recovery time of FDs may have different relations with energy: two of them exhibit a correlation pattern and one does not (Figure 12 right). Our theoretical modelling indicates that the "correlation" events can be likely associated with the head-on FD, while the "no-correlation" one can be attributed to an edge-on FD.

4.7 Exotics searches: fractionally-charged particles

Search for Fractionally-Charged Particles (FCPs) – hypothetical smoking gun signatures predicted in some extensions of the Standard Model gauge group was published by DAMPE in 2022 [50] and presented at this conference [51]. Until recently, most of the FCP searches were carried out by

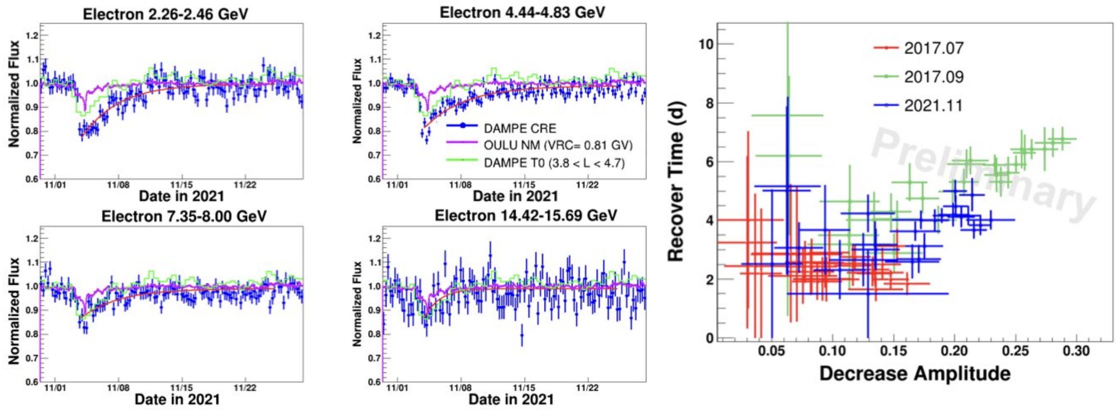

Figure 12: Left: fit result of FD observed by DAMPE in November 2021 in 4 different energy bins. Violet line corresponds to the Oulu NM normalized counts, red line represents the best fit result of DAMPE CRE. Right: relation between decrease amplitude and the recovery time for the three FD events observed by DAMPE. Figures from [49].

ground-based experiments at high altitudes, requiring FCP energies of few hundred GeV and higher. Other FCP searches were carried out by AMS-01 [52] and BESS [53]. DAMPE is sensitive to much lower FCP energies compared to ground-based detectors. It puts the most stringent constraint on FCP flux, more than two orders of magnitude lower than the previous baloon- and space-based experiments, at a few GeV.

4.8 Hadronic cross sections

The theoretical description of hadronic interactions is a key component of the energy reconstruction of hadronic CR in DAMPE and similar calorimetric experiments. At this conference a method for inelastic hadronic cross section measurement with DAMPE was presented [54], based on the application of machine learning techniques for particle tagging [33]. Preliminary results were demonstrated for the cross sections of proton/helium inelastic interactions against BGO as a target material (Figure 13).

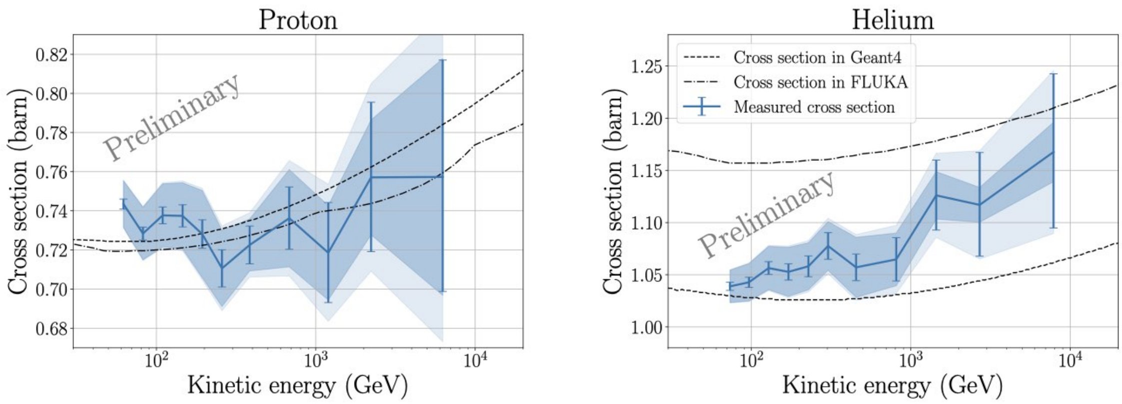

Figure 13: Measurement of the inelastic hadronic cross section of proton and helium on $Bi_4Ge_3O_{12}$. Figure from [54].

A good agreement with the theoretical prediction can be observed for the rather well-studied proton cross sections, which is indicative of the validity of the demonstrated approach. At the same time, the results show an interesting insight into the helium cross sections, indicating that data favours the theoretical predictions adopted in the GEANT4 simulation package, below ~TeV. At higher energies, the measured cross sections appear to increase towards the FLUKA prediction, although the statistical uncertainties are relatively high in order to claim a definitive trend. In addition, preliminary measurements of carbon and oxygen cross sections at BGO were presented as well [55].

4.9 Gamma rays

DAMPE is capable of detecting gamma rays starting at ~2 GeV with an effective acceptance of about 0.18 $m^2 \cdot sr$. Over the past years, the understanding of the instrument response with respect to gamma rays improved significantly [56–60]. The entire gamma-ray sky was covered 15 times since the start of the mission, with about 300 thousand gamma rays collected (Figure 14). For a comprehensive review of DAMPE gamma-ray physics and related instrument calibration, presented at the conference, see [61].

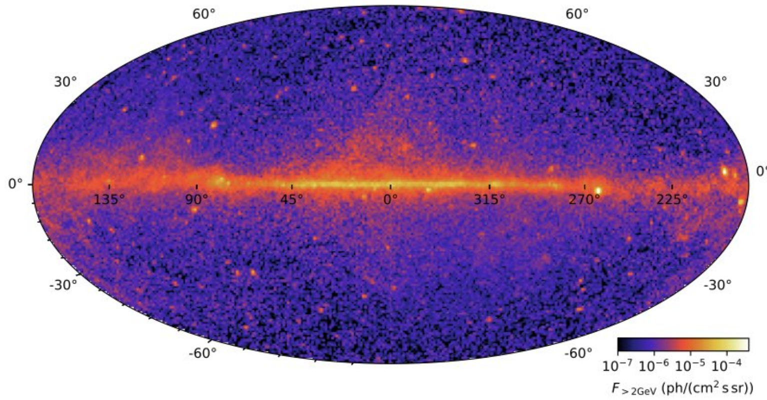

Figure 14: The map of the integrated gamma-ray flux above 2 GeV derived with 7.2 years of DAMPE data. Figure from [61].

Gamma ray physics presented at this conference includes the observation of point/transient sources, the study of the Galactic center and Fermi bubbles, as well as the search for dark matter line signatures in the diffuse gamma-ray spectrum. As of now DAMPE has detected 248 sources with the TS value over 25. Among those are 175 active galactic nuclei, 46 pulsars, 10 supernovae remnants or pulsar wind nebulae, 6 binaries, and 11 unassociated [62].

In [63], the study of the Galactic Center Excess (GCE) is presented. The GCE is a 10–15° spherical excess in the galactic center, which peaks at about 2 GeV. DAMPE has established the GCE with 7.9σ significance based on 7.2 years of data, in the energy range between 2 GeV and 31.6 GeV. In addition, Fermi bubbles (FB) – about 40° structures that extend below and above the galactic plane are also detected by DAMPE with high significance, 17.8σ, based on 6 years of data [61]. Overall, the GCE and FB spectra match well with the Fermi-LAT results [64, 65].

Finally, the search for the gamma-ray line signatures that may arise in the dark matter annihilation or decay was published in 2022 [41]. Thanks to the excellent energy resolution, DAMPE provides the most stringent constraints on dark matter decay lifetime below 100 GeV (Figure 15).

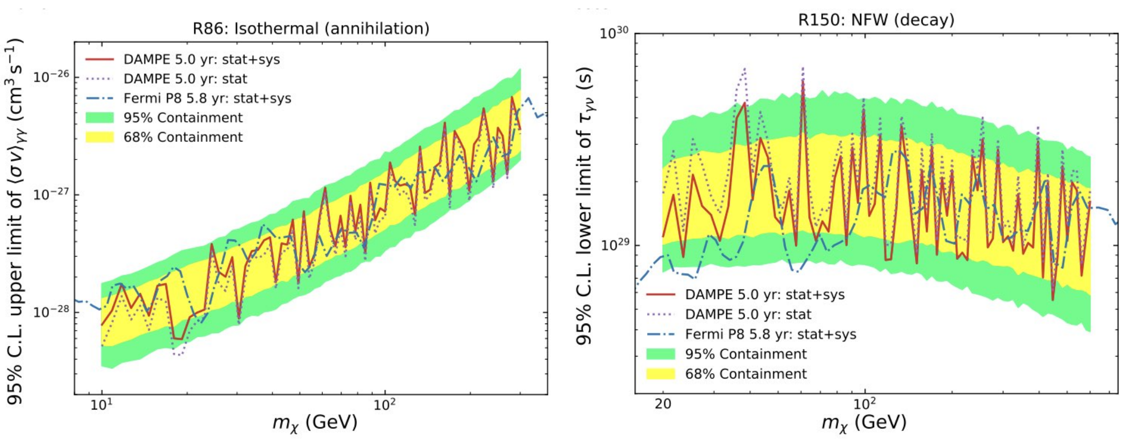

Figure 15: The constraints on dark matter annihilation cross section (left) and decay lifetime (right) derived from the gamma-ray line search with DAMPE. See [41] and [61] for the detail description.

5. Summary

The DAMPE instrument demonstrates excellent performance and stability after more than 7.5 years of data collection. Its thick $32X_0$ calorimeter provides outstanding energy resolution, which, combined with a relatively large instrument acceptance, allows for precise probing of leptonic and hadronic cosmic rays at the highest energies reachable by direct-detection experiments in space. A wealth of physics results has been already published by DAMPE, including the detection of a TeV break in the cosmic-ray electron spectrum, the observation of a softening structure in primary hadronic cosmic rays at the highest energies, and a remarkable 100 GeV hardening in secondary-to-primary cosmic ray ratios. An active program is underway on extending the analysis to higher energies with more advanced analysis techniques: improved results for the proton and the helium spectra were presented with the higher data statistics, based on the recently developed machine learning data reconstruction approach. The spectra indicate a charge-dependent behaviour of the hardening and the softening structures in the proton and helium fluxes. Furthermore, a combined proton+helium spectrum was presented up to 316 TeV kinetic energy, submitted for publication. It establishes a link between space- and ground-based cosmic-ray experiments, at the same time hinting towards a possible interesting structure beyond 100 TeV. The collaboration is actively working on the spectral analysis of the cosmic-ray secondaries, CNO group and beyond. A preliminary measurement of the combined CNO spectrum confirms a spectral hardening structure in primary cosmic rays at about few hundred GeV per nucleon and gives a hint of a possible softening at ~100 TeV kinetic energy. The physics program of DAMPE also includes searches for exotic signatures, such as fractionally-charged particles. Furthermore, excellent energy resolution allows DAMPE to probe the imprints of energetic solar effects on galactic cosmic rays, providing interesting new insights into the spectral/time behavior of the Forbush decrease effect. First results on the measurement of hadronic cross sections for proton, helium, carbon and oxygen, against the BGO target material were presented as well, which will have a very significant impact on the future measurement of hadronic cosmic rays. Finally, a rich gamma-ray program of DAMPE includes the detection of multiple sources, a solid confirmation of the Galactic Center Excess and the Fermi bubbles, and provides the most stringent constraints on dark matter decay lifetime below 100 GeV.

6. Acknowledgements

The DAMPE mission was funded by the strategic priority science and technology projects in space science of Chinese Academy of Sciences (CAS). In China, the data analysis was supported by the National Key Research and Development Program of China (No. 2022YFF0503302) and the National Natural Science Foundation of China (Nos. 12103094, 12220101003, 11921003, 11903084, 12003076 and 12022503), the CAS Project for Young Scientists in Basic Research (No. YSBR061), the Youth Innovation Promotion Association of CAS, the Young Elite Scientists Sponsorship Program by CAST (No. YESS20220197), and the Program for Innovative Talents and Entrepreneur in Jiangsu. In Europe, the activities and data analysis are supported by the Swiss National Science Foundation (SNSF), Switzerland, the National Institute for Nuclear Physics (INFN), Italy, and the European Research Council (ERC) under the European Union's Horizon 2020 research and innovation programme (No. 851103).

References

[1] J. Chang, et al., Astropart. Phys. (2017). doi:10.1016/j.astropartphys.2017.08.005.
[2] Y. Yu, et al., Astropart. Phys. (2017). doi:10.1016/j.astropartphys.2017.06.004.
[3] P. Azzarello, et al., NIM A (2016). doi:10.1016/j.nima.2016.02.077.
[4] Y. Wei, et al. (2019). doi:10.1016/j.nima.2018.12.036.
[5] Y.-Y. Huang, et al., Res. Astron. Astrophys. (2020). doi:10.1088/1674-4527/20/9/153.
[6] A. Tykhonov, et al., J. Phys. Conf. Ser. (2017). doi:10.1088/1742-6596/898/4/042031.
[7] C. Wang, et al., Chin. Phys. C (2017). doi:10.1088/1674-1137/41/10/106201.
[8] J. Allison, et al., NIM A (2016). doi:10.1016/j.nima.2016.06.125.
[9] T. Böhlen, et al., Nucl. Data Sheets (2014). doi:10.1016/j.nds.2014.07.049.
[10] J. J. Zang, et al., PoS ICRC2017 (2018) 197. doi:10.22323/1.301.0197.
[11] J. J. Zang, et al., PoS ICRC2023 (2023) 129.
[12] Z.-F. Chen, et al., NIM A (2023). doi:10.1016/j.nima.2023.168470.
[13] Y. Wei, et al., IEEE Trans. Nucl. Sci. (2020). doi:10.1109/TNS.2020.2989191.
[14] C. Zhao, et al., PoS ICRC2023 (2023) 163. doi:10.22323/1.444.0163.
[15] M. Ding, et al., Res. Astron. Astrophys. (2019). doi:10.1088/1674-4527/19/3/47.
[16] T. Dong, et al., Astropart. Phys. (2019). doi:10.1016/j.astropartphys.2018.10.001.
[17] P.-X. Ma, et al., Res. Astron. Astrophys. (2019). doi:10.1088/1674-4527/19/6/82.
[18] J. B. Birks, Proc. Phys. Soc. A (1951). doi:10.1088/0370-1298/64/10/303.
[19] A. Tykhonov, et al., NIM A (2019). doi:10.1016/j.nima.2018.06.036.
[20] A. Tykhonov, et al., NIM A (2018). doi:10.1016/j.nima.2018.02.105.
[21] T. Kobayashi, et al., Astrophys. J. (2004). doi:10.1086/380431.
[22] DAMPE collaboration, Nature 552 (2018). doi:10.1038/nature24475.
[23] A. Archer, et al., Phys. Rev. D (2018). doi:10.1103/PhysRevD.98.062004.
[24] O. Adriani, et al., Phys. Rev. Lett. (2018). doi:10.1103/PhysRevLett.120.261102.
[25] D. Droz, et al., JINST (2021). doi:10.1088/1748-0221/16/07/P07036.

[26] Z. Xu, et al., Universe (2022). doi:10.3390/universe8110570.

[27] E. Putti-Garcia, et al., PoS ICRC2023 (2023) 130. doi:10.22323/1.444.0130.

[28] DAMPE collaboration, Sci. Adv. (2019). doi:10.1126/sciadv.aax3793.

[29] M. Aguilar, et al. (2015). doi:10.1103/PhysRevLett.114.171103.

[30] DAMPE collaboration, Phys. Rev. Lett. (2021). doi:10.1103/PhysRevLett.126.201102.

[31] C. Yue, et al., NIM A (2020). doi:10.1016/j.nima.2020.164645.

[32] A. Ruina, et al., PoS ICRC2023 (2023) 170. doi:10.22323/1.444.0170.

[33] A. Tykhonov, et al., Astrpt. Phys. (2023). doi:10.1016/j.astropartphys.2022.102795.

[34] M. Stolpovskiy, et al., JINST 17 (06) (2022). doi:10.1088/1748-0221/17/06/p06031.

[35] DAMPE collaboration (2023). arXiv:2304.00137.

[36] F. Alemanno, et al., PoS ICRC2023 (2023) 138. doi:10.22323/1.444.0138.

[37] A. Parenti, et al., PoS ICRC2023 (2023) 137. doi:10.22323/1.444.0137.

[38] Y.-F. Wei, et al., PoS ICRC2023 (2023) 165. doi:10.22323/1.444.0165.

[39] M. Stolpovskiy, et al., PoS ICRC2023 (2023) 168. doi:10.22323/1.444.0168.

[40] P.-X. Ma, et al., PoS ICRC2023 (2023) 132.

[41] DAMPE collaboration, Sci. Bull. (2022). doi:10.1016/j.scib.2022.10.002.

[42] Y. Chuan, et al., PoS ICRC2023 (2023) 159. doi:10.22323/1.444.0159.

[43] R. H. Kraichnan, The Physics of Fluids 8 (7) (1965) 1385–1387.

[44] A. N. Kolmogorov, Numbers. In Dokl. Akad. Nauk SSSR 30 (1941) 301.

[45] P. Mertsch, et al., Phys. Rev. D (2021). doi:10.1103/physrevd.104.103029.

[46] N. Kawanaka, S. Yanagita, PRL (2018). doi:10.1103/PhysRevLett.120.041103.

[47] S. E. Forbush, Phys. Rev. (1937). doi:10.1103/PhysRev.51.1108.3.

[48] DAMPE collaboration, Astrophys. J. Lett. (2021). doi:10.3847/2041-8213/ac2de6.

[49] W.-H. Li, et al., PoS ICRC2023 (2023) 1311. doi:10.22323/1.444.1311.

[50] DAMPE collaboration, Phys. Rev. D (2022). doi:10.1103/PhysRevD.106.063026.

[51] C.-M. Liu, et al., PoS ICRC2023 (2023) 149. doi:10.22323/1.444.0149.

[52] C. Sbarra, et al. (2003). arXiv:astro-ph/0304192.

[53] H. Fuke, et al., Advances in Space Research (2008). doi:10.1016/j.asr.2007.02.042.

[54] P. Coppin, et al., PoS ICRC2023 (2023) 142. doi:10.22323/1.444.0142.

[55] E.-H. Xu, et al., PoS ICRC2023 (2023) 161. doi:10.22323/1.444.0161.

[56] Z.-L. Xu, et al., Front. Phys. (Beijing) (2022). doi:10.1007/s11467-021-1121-6.

[57] Y.-X. Cui, et al., NIMA A (2023). doi:10.1016/j.nima.2022.167670.

[58] W. Jiang, et al., Res. Astron. Astrophys. (2020). doi:10.1088/1674-4527/20/6/92.

[59] K.-K. Duan, et al., Res. Astron. Astrophys. (2019). doi:10.1088/1674-4527/19/9/132.

[60] Z.-L. Xu, et al., Res. Astron. Astrophys. (2018). doi:10.1088/1674-4527/18/3/27.

[61] Z.-Q. Shen, et al., PoS ICRC2023 (2023) 670. doi:10.22323/1.444.0670.

[62] K.-K. Duan, et al., PoS ICRC2023 (2023) 669. doi:10.22323/1.444.0669.

[63] Z.-Q. Shen, et al., PoS ICRC2023 (2023) 671.

[64] T. Daylan, et al., Phys. Dark Univ. (2016). doi:10.1016/j.dark.2015.12.005.

[65] M. Ackermann, et al., Astrophys. J. (2014). doi:10.1088/0004-637X/793/1/64.

Full Authors List: DAMPE Collaboration

F. Alemanno[1,2*], C. Altomare[3], Q. An[4,5†], P. Azzarello[6], F. C. T. Barbato[1,2], P. Bernardini[7,8], X. J. Bi[9,10], I. Cagnoli[1,2], M. S. Cai[11,12], E. Casilli[7,8], E. Catanzani[13], J. Chang[11,12], D. Y. Chen[11], J. L Chen[14], Z. F. Chen[11,12], Z.X. Chen[14], P. Coppin[6], M. Y. Cui[11], T. S. Cui[15], Y. X. Cui[11,12], I. De Mitri[1,2], F. de Palma[7,8], A. Di Giovanni[1,2], M. Di Santo[1,2], Q. Ding[11,12], T. K. Dong[11], Z. X. Dong[15], G. Donvito[3], D. Droz[6], J. L. Duan[14], K. K. Duan[11], R. R. Fan[10], Y. Z. Fan[11,12], F. Fang[14], K. Fang[10], C. Q. Feng[4,5], L. Feng[11], M. Fernandez Alonso[1,2], J. M. Frieden[6‡], P. Fusco[3,16], M. Gao[10], F. Gargano[3], E. Ghose[7,8], K. Gong[10], Y. Z. Gong[11], D. Y. Guo[10], J. H. Guo[11,12], S. X. Han[15], Y. M. Hu[11], G. S. Huang[4,5], X. Y. Huang[11,12], Y. Y. Huang[11], M. Ionica[13], L. Y. Jiang[11], W. Jiang[11], Y. Z. Jiang[13], J. Kong[14], A. Kotenko[6], D. Kyratzis[1,2§], S. J. Lei[11], W. L. Li[15], W. H. Li[11,12], X. Li[11,12], X. Q. Li[15], Y. M. Liang[15], C. M. Liu[4,5], H. Liu[11], J. Liu[14], S. B. Liu[4,5], Y. Liu[11], F. Loparco[3,16], C. N. Luo[11,12], M. Ma[15], P. X. Ma[11], T. Ma[11], X. Y. Ma[15], G. Marsella[7,8¶], M. N. Mazziotta[3], D. Mo[14], X. Y. Niu[14], X. Pan[11,12], A. Parenti[1,2], W. X. Peng[10], X. Y. Peng[11], C. Perrina[6‖], E. Putti-Garcia[6], R. Qiao[10], J. N. Rao[15], A. Ruina[6], Z. Shangguan[15], W. H. Shen[15], Z. Q. Shen[11], Z. T. Shen[4,5], L. Silveri[1,2], J. X. Song[15], M. Stolpovskiy[6], H. Su[14], M. Su[17], H. R. Sun[4,5], Z. Y. Sun[14], A. Surdo[8], X. J. Teng[15], A. Tykhonov[6], J. Z. Wang[10], L. G. Wang[15], S. Wang[11], X. L. Wang[4,5], Y. F. Wang[4,5], Y. Wang[4,5], Y. Z. Wang[11], D. M. Wei[11,12], J. J. Wei[11], Y. F. Wei[4,5], D. Wu[10], J. Wu[11,12**], L. B. Wu[1,2], S. S. Wu[15], X. Wu[6], Z. Q. Xia[11], E. H. Xu[4,5], H. T. Xu[15], J. Xu[11], Z. H. Xu[11,12], Z. Z. Xu[4,5], Z. L. Xu[11], G. F. Xue[15], H. B. Yang[14], P. Yang[14], Y. Q. Yang[14], H. J. Yao[14], Y. H. Yu[14], G. W. Yuan[11,12], Q. Yuan[11,12], C. Yue[11,12], J. J. Zang[11††], S. X. Zhang[14], W. Z. Zhang[15], Yan Zhang[11], Y. P. Zhang[14], Yi Zhang[11,12], Y. J. Zhang[14], Y. Q. Zhang[11], Y. L. Zhang[4,5], Z. Zhang[11], Z. Y. Zhang[4,5], C. Zhao[4,5], H. Y. Zhao[14], X. F. Zhao[15], C. Y. Zhou[15], and Y. Zhu[15]

[1]Gran Sasso Science Institute (GSSI), I-67100 L'Aquila, Italy
[2]Istituto Nazionale di Fisica Nucleare (INFN) - Laboratori Nazionali del Gran Sasso, I-67100 Assergi, L'Aquila, Italy
[3]Istituto Nazionale di Fisica Nucleare (INFN), Sezione di Bari, I-70126 Bari, Italy
[4]State Key Laboratory of Particle Detection and Electronics, University of Science and Technology of China, Hefei 230026, China
[5]Department of Modern Physics, University of Science and Technology of China, Hefei 230026, China
[6]Department of Nuclear and Particle Physics, University of Geneva, CH-1211 Geneva, Switzerland
[7]Dipartimento di Matematica e Fisica E. De Giorgi, Università del Salento, I-73100 Lecce, Italy
[8]Istituto Nazionale di Fisica Nucleare (INFN) - Sezione di Lecce, I-73100 Lecce, Italy
[9]University of Chinese Academy of Sciences, Beijing 100049, China
[10]Institute of High Energy Physics, Chinese Academy of Sciences, Beijing 100049, China
[11]Key Laboratory of Dark Matter and Space Astronomy, Purple Mountain Observatory, Chinese Academy of Sciences, Nanjing 210023, China
[12]School of Astronomy and Space Science, University of Science and Technology of China, Hefei 230026, China
[13]Istituto Nazionale di Fisica Nucleare (INFN), Sezione di Perugia, I-06123 Perugia, Italy
[14]Institute of Modern Physics, Chinese Academy of Sciences, Lanzhou 730000, China
[15]National Space Science Center, Chinese Academy of Sciences, Beijing 100190, China
[16]Dipartimento di Fisica "M. Merlin" dell'Università e del Politecnico di Bari, I-70126 Bari, Italy
[17]Department of Physics and Laboratory for Space Research, the University of Hong Kong, Hong Kong SAR, China

[*]Now at Dipartimento di Matematica e Fisica E. De Giorgi, Università del Salento, I-73100, Lecce, Italy
[†]Deceased
[‡]Now at Institute of Physics, Ecole Polytechnique Fédérale de Lausanne (EPFL), CH-1015 Lausanne, Switzerland
[§]Now at Department of Nuclear and Particle Physics, University of Geneva, CH-1211 Geneva, Switzerland
[¶]Now at Dipartimento di Fisica e Chimica "E. Segrè", Università degli Studi di Palermo, I-90128 Palermo, Italy
[‖]Now at Institute of Physics, Ecole Polytechnique Fédérale de Lausanne (EPFL), CH-1015 Lausanne, Switzerland
[**]Deceased
[††]Also at School of Physics and Electronic Engineering, Linyi University, Linyi 276000, China.